Tuning the focusing spot of plasmonic nanolens by aspect ratio under linear polarization

Shuiyan Cao (曹水艳)[1,2], Weixing Yu (鱼卫星)[1*], Cheng Wang (王 成)[1], and Yongqi Fu (付永启)[3]**

[1]*State Key Laboratory of Applied Optics, Changchun Institute of Optics, Fine Mechanics and Physics, Chinese Academy of Sciences, Changchun, Jilin 130033, China*

[2]*University of Chinese Academy of Sciences, Beijing 10049, China*

[3]*School of Physical Electronics, University of Electronic Science and Technology of China, Chengdu 610054, China*

[*]*Corresponding author: yuwx@ciomp.ac.cn;* [**]*corresponding author: yqfu@uestc.edu.cn*

Received September 21, 2013; accepted November 28, 2013; posted online January 8, 2014

A new plasmonic nanolens that can be tuned by varying the circular structure into an elliptical annulus and the aspect ratio from 1 to 0.1 and 1 to 2, respectively, is proposed. Using the rigorous finite-difference and time-domain algorithm, we find that when the aspect ratio ranges from 1 to 0.1, a good linear relationship exists between the aspect ratio and focusing spot size at the full-width at half-maximum in the x- and y-directions, respectively. The corresponding calculated FWHM ranges from 96×126 (nm) to 15×52 (nm) (Full Width at Half Maximum).

OCIS codes: 240.6680, 310.6628, 000.4430, 350.5730.

doi: 10.3788/COL201412.012401.

Surface plasmon polaritons (SPPs) have elicited considerable research attention for several decades, with applications ranging from high-density optical data storage[1,2], probes via scanning near-field optical microscopy[3], light focusing[4], sensors[5], and plasmonic devices that can be used for immunoassays[6,7]. Researchers have focused on SPPs-based optical devices because they can achieve sub-wavelength resolutions for applications in nanolithography[8]. Numerous approaches to obtain super-resolution are based on plasmonic optical devices. For instance, Wood *et al.*[9] suggested a layered metal-dielectric system to obtain subwavelength resolutions, and Tsai *et al.*[10] studied the super-resolution near-field structure of AgO_x type. Additionally, several different types of nanolenses have been proposed for achieving super-solutions such as depth-tuned structure[11], width-tuned structure[12], circular grating-based metallic structure[13–16], and elliptical nanopinhole structure[17]. In this letter, we present a new structure on based on a metallic periodic structure. The influence on superfocusing on this structure has been systematically studied, and positive results regarding an elliptical focusing spot in the propagation distance from the exit plane of the nanolens in free space ($Z = 20$ nm) have been derived[13].

Here, we tuned the circular structure of the nanolens into an elliptical structure. The finite-difference and time-domain (FDTD) (Lumerical Inc.) algorithm was used in the computational numerical calculation[18]. Our results demonstrate that a good linear relationship exists during the varying of the aspect ratio between the length of the x- and y-axes of the elliptical nanolens. In detail, the aspect ratio is found to be linearly proportional to the size of the central focusing spot, which lies in the near-field region approximately 20 nm within working distance. We believe that these results can greatly improve nanolithography because we can control the shape of the focusing spot by adjusting the aspect ratio of the elliptical structure.

The designed Ag elliptical ring nanolens with $d = 75$ nm in thickness is shown in Fig. 1. The dielectric constant of Ag is –9.28+0.79i. An elliptical hole with 100-nm constant diameter in the x-direction is etched at center of this lens. Five concentric elliptical rings were constructed with the period of $\wedge = 490$ nm and constant ring width of $w = 50$ nm in the x-direction. This chosen period was equal to the wavelength of SPP (λ_{SPP}) to meet the condition of SPP resonance for the periodic structure. The wavelength of the SPPs was calculated based on the following equation: $\lambda_{\mathrm{SPP}} = \lambda_0 \sqrt{\frac{\varepsilon_{\mathrm{d}} + \varepsilon'_{\mathrm{m}}}{\varepsilon'_{\mathrm{m}} \varepsilon_{\mathrm{d}}}}$ (λ_0 represents the incident wavelength, ε_{d} and $\varepsilon'_{\mathrm{m}}$ represent the dielectric constant of dielectric and metal constant respectively). Here, the incident wavelength of 514 nm was used, and λ_{SPP} was thus equal to 490 nm. The incident light was a linearly x-polarized plane wave with an amplitude of 1 and propagated along the positive z-direction. To meet the condition of plasmonic resonance, we kept constant the period and ring width, as well as the elliptical hole length in the x-direction. By turning the aspect ratio between x- (short) axis and y- (long) axes of the elliptical ring as well as the elliptical hole, we constructed the structure as shown in Figs. 1(a) and 1(b). These figures (Figs. 1(a) and 1(b)) represent structures with aspect ratios varying from 1 to 0.1 and 1 to 2, respectively. Figure 1(c) shows the side view of our designed structures.

Simulation time and mesh size were set as 200 fs and $\Delta x = \Delta y = \Delta z = 5$ (nm) respectively in our three-dimensional (3D) calculation. To reduce spurious reflections from the computational window edges, the use of the perfectly matched layer (PML) boundary condition is indispensable. Accordingly, symmetry and anti-symmetry boundary conditions were set to accelerate simulation speed because of the symmetry of the structure.

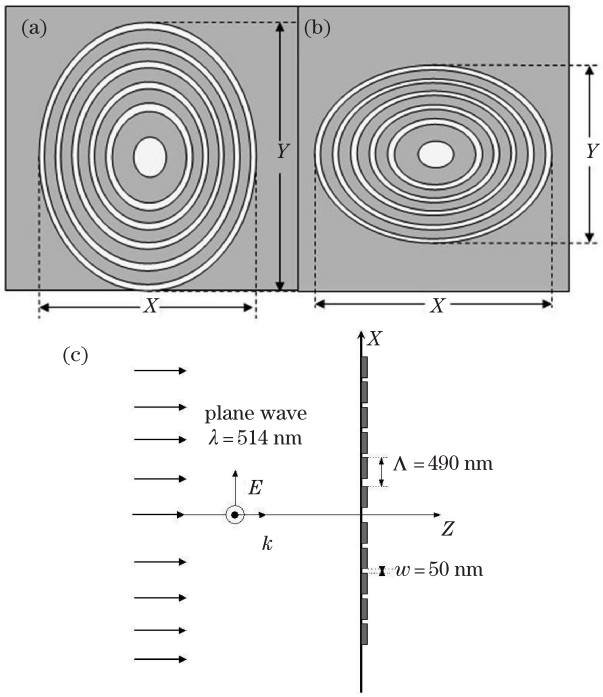

Fig. 1. Schematic of designed plasmonic nanolens. (a) Aspect ratios from 1 to 0.1; (b) aspect ratios from 1 to 2; (c) side view of the structure.

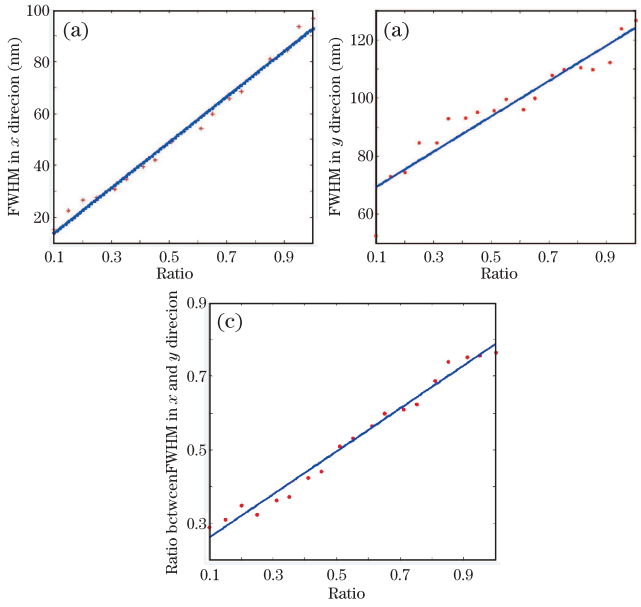

Fig. 2. Linear relationship between aspect ratio and FWHM in the x-axis; (b) linear relationship between aspect ratio and FWHM in the y-axis; (c) linear relationship between aspect ratio and ratio of FWHM in the x- and y-axes.

Our numerical calculations reveal a good linear relationship when the aspect ratio changes from 1 to 0.1 (Fig. 2). Figure 2(a) indicates that the aspect ratio is linearly proportional to Full Width at Half Maximum (FWHM) of focusing spot in the x-direction. Figure 2(b) shows that when the aspect ratio is 0.1, the FWHM in the y-direction is 52 nm, which does not lie near the linear line. A linear relationship was also observed in other aspect ratios between the aspect ratio and FWHM in the y-direction. Additionally, Fig. 2(c) also indicates a good linear relationship between the aspect ratio of the structure and the ratio of FWHM between the x- and y-directions. The correlation coefficients calculated in Figs. 2(a)–2(c) are 0.99, 0.95, and 0.99, respectively, which are all almost near 1. Evidently, the linear relationship has a strong correlation.

Figure 3 shows the E_x-field distribution at $Z = 20$ nm for different aspect ratios along the x-axis (Fig. 3(a)) and y-axis (Fig. 3(b)), respectively. When the aspect ratio gradually decreases, the coupling effect improves. This phenomenon is most apparent when the aspect ratio is 0.1; it manifests extremely strong amplitude in the E_x-field, becoming greater than 50 with a focusing size of 15×52 (nm). We also plot the E_x-field distribution along the x- and y-axis when the ratio is 0.1 under the mesh size of $\Delta x = \Delta y = \Delta z = 2$ (nm), as shown in Fig. 4. The focusing size shown in Fig. 4 is 18×56 (nm). When this result is compared with the focusing size of 15×52 (nm), it increases in the x-direction; to reduce simulation time, the mesh size of $\Delta x = \Delta y = \Delta z = 5$ (nm) was used here.

When the aspect ratio changes from 1 to 0.1, a good linear relationship is observed. As regards aspect ratios larger than 1, the values range from 1 to 2, which means that our structure can change shape into the pattern shown in Fig. 1(b). Figure 5 shows that the variation rule is irregular compared with the good linear relationship that occurred in the aspect ratio changing from 1 to 0.1, as mentioned above. This finding indicates that FWHM fluctuates and is unstable, especially in the y-direction.

Figures 6(a) and (b) show the E_x-field distribution along x- and y-directions for different aspect ratios. As the aspect ratio increases, the intensity of focusing spot decreases and focusing effect degrades accordingly. When the aspect ratio is 2, the central intensity of E_x in the x-direction is almost zero.

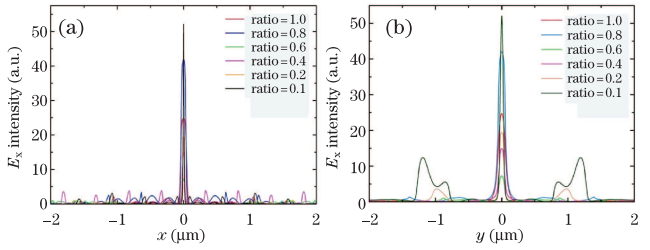

Fig. 3. (Color online) E_x-field distributions for different aspect ratios: (a) in the x-direction of the focusing spot, and (b) in the y-direction of the focusing spot.

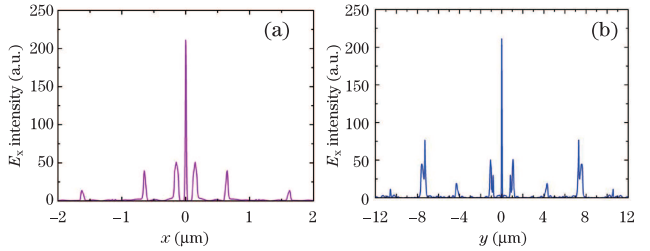

Fig. 4. (a) E_x-field distribution in the x-axis when the aspect ratio is 0.1 under the mesh size of $\Delta x = \Delta y = \Delta z = 2$ (nm). (b) E_x-field distribution in the y-axis when the aspect ratio is 0.1 under the mesh size of $\Delta x = \Delta y = \Delta z = 2$ (nm).

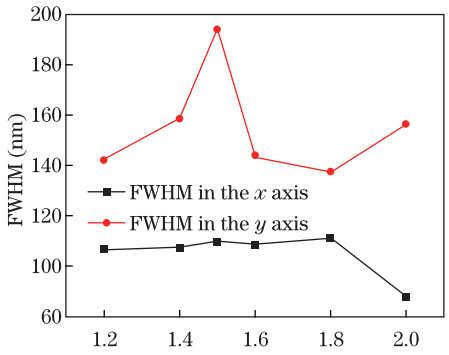

Fig. 5. FWHM distribution in the x- and y-axes for different aspect ratios.

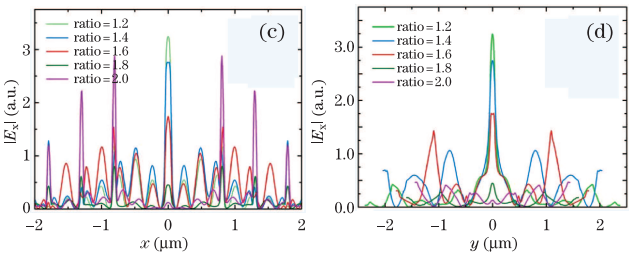

Fig. 6. (Color online) E_x distributions for different aspect ratios: (a) in the x-axis, and (b) in the y-axis.

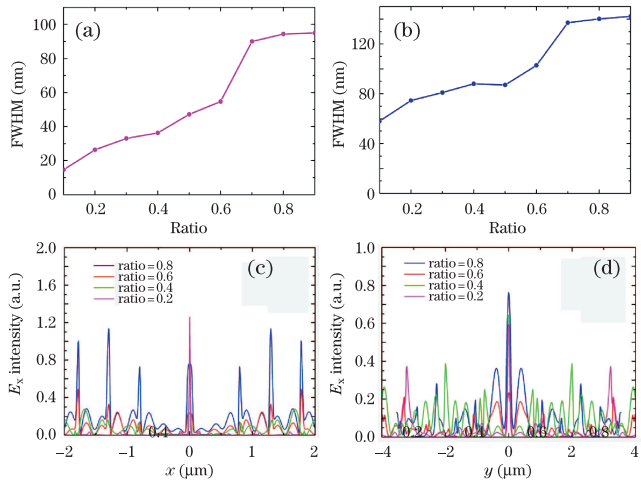

Fig. 7. (Color online) Relationship between aspect ratio and FWHM of focusing spot (a) in the x-direction under y-polarization incident light and (b) in the y-direction under y-polarization incident light. E_x-field distribution for different ratios (c) along the x-direction under y-polarization incident light and (d) along the y-direction under y-polarization incident light.

We attribute the different phenomena occurring in the cases of aspect ratios both greater than and less than 1 to the x-polarization incident wavelength. Figures 7(a) and 7(b) show the variation in FWHM of the focusing spot in the x- and y-directions when the ratio is changed from 0.9 to 0.1 under the y-polarization incident light. As the ratio decreases, FWHM in the x and y-directions also decrease in general. Similar to the results shown in Figs. 2 and 5, the structure of Fig. 1(a) can minimize the size of the focusing spot when its aspect ratios decrease, as opposed to the structure of Fig. 1(b). Moreover, Figs. 7(a) and 7(b) do not present a good linear relationship, as shown in Fig. 2. Thus, x-polarization is important for a good linear relationship.

Additionally, E_x-field distribution for different ratios along the x and y-direction under the y-polarization incident light were also presented in Figs. 7(c) and (d). We can see that although the FWHM of focusing spot is similar to the result in Fig. 2, E_x-field distribution is different because the E_x intensity in Figs. 7(c) and 7(d) is relatively low.

Figure 8 shows the variation of the shape of focusing spot when the aspect ratio gradually changes. Figure 6 indicates that when the aspect ratio is larger than 1.6, the intensity is relatively small. Thus, the aspect ratio varies from 1.4, 1.2, 1, 0.8, 0.6, 0.4, 0.2, and

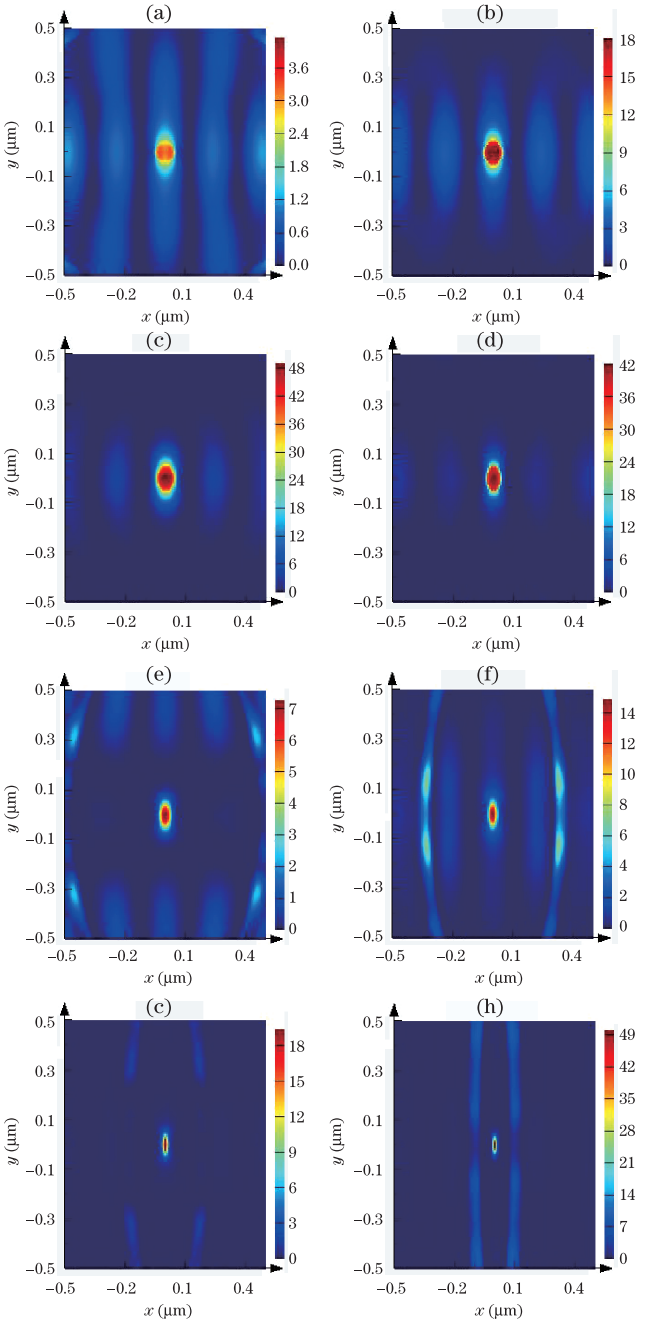

Fig. 8. E-field intensity distributions of the focusing spot with various aspect ratios: (a) 1.4, (b) 1.2, (c) 1, (d) 0.8, (e) 0.6, (f) 0.4, (g) 0.2, and (h) 0.1.

0.1, and corresponding results are shown in Figs. 8(a) to (h), respectively. The size of the focusing spot is 96×126 (nm) when the aspect ratio is 1; this is not symmetrical, which has been indicated elsewhere[13]. Additionally, the size gradually changes as the aspect ratio varies. The elliptical spot becomes long and thin when the aspect ratio becomes 0.1. This is practically a line with a size of 15×52 (nm), as shown in Fig. 8(h). In this case, strong E-field intensity occurs. Additionally, the E-field distribution at the $X - Z$ planes for different aspect ratios of 1, 0.7, 0.5, and 0.1, respectively, are shown in Fig. 9. As the aspect ratios increase, the focusing effect on the $X - Z$ plane improves. The distribution of the E field in the x-axis becomes narrower, especially when the ratio is 0.1; this is practically a line distribution, and corresponds to Fig. 8(h). Moreover, Fig. 9 also indicates that this is characteristic of near field focusing phenomenon, because the focusing far field cannot be observed. This may be attributed to the small size effect, in which x-polarization-induced SPPs propagating along x-axis are important for enhanced transmission. Subsequently, a "hot spot" is generated by the transmission under diffractive wavelet interference[19].

As regards the significance of our results, values beyond diffraction limits are usually defined by the dimensions of the spot of the coupling beam at less than half of the wavelength. However, in our case, when the aspect ratio is 0.1, the size of the spot is 15×52 (nm), which is less than $\lambda/10$. Compared with a previous study, which indicates that resolutions can reach $\lambda/6$, our results are advantageous[20]. Additionally, our results may be useful for nanolithography because previous studies have shown that via radially polarized light, circular focusing spots may be obtained[21,22]. Our results demonstrate that linear relationships occur when the aspect ratio varies from 1 to 0.1. We can obtain any size of the elliptical focusing spot in the range of 96×126 (nm) to 15×52 (nm) if required.

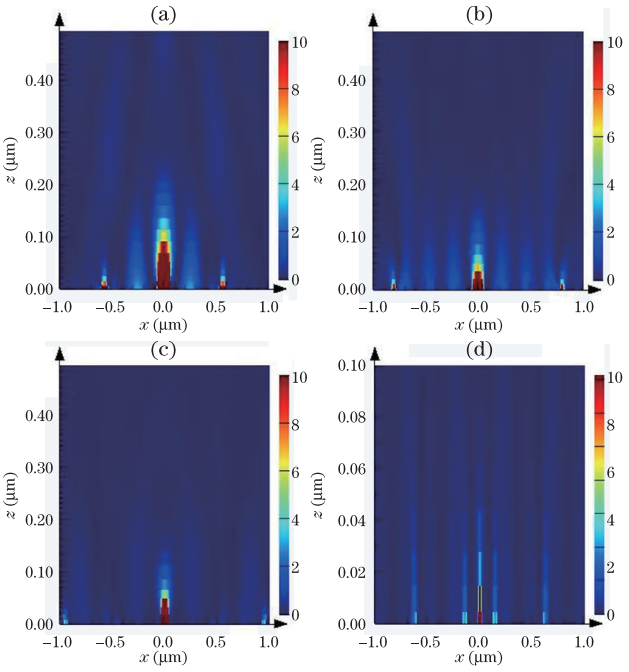

Fig. 9. E-field distribution at the $X - Z$ plane for different aspect ratios: (a) 1, (b) 0.7, (c) 0.5, and (d) 0.1.

In conclusion, we used rigorous FDTD to systematically study the focusing effect when adjusting the circular plasmonic nanolens into elliptical plasmonic nanolens. When the aspect ratio varies from 1 to 0.1, a good linear relationship is observed in terms of the ratio and FWHM of focusing spot at $Z = 20$ nm from exit plane in the x- and y-directions, respectively. The size of the elliptical focusing spot changes from 96×126 (nm) to 15×52 (nm). However, this linear phenomenon does not exist in the situation when the aspect ratio is ranging from 1 to 2. We believe that our findings have practical applications in the fields of nano-photolithography, data storage, and sensing.

This work was supported by the National Natural Science Foundation of China (Nos. 90923036, 60977041, 60877021, and 61077010), the 100 Talents Program of Chinese Academy of Sciences, and the Ministry of Science and Technology of China (No. 2010DFR10660).

References

1. P. Zijlstra, J. W. M. Chon, and M. Gu, Nature **459,** 410 (2009).
2. H. Ditlbacher, B. Lamprecht, A. Leitner, and F. R. Aussenegg, Opt. Lett. **25,** 563 (2000).
3. T. J. Antosiewicz, P. Wrobel, and T. Szoplik, Plasmonics **6,** 11 (2011).
4. W. L. Barnes, A. Dereus, and T. W. Ebbesen, Nature **424,** 824 (2003).
5. Y. Chen, R. Zheng, Y. Lu, P. Wang, and H. Ming, Chin. Opt. Lett. **9,** 100605 (2011).
6. L. Zhou, F. Ding, H. Chen, W. Ding, W. Zhang, and S. Y. Chou, Anal. Chem. **84,** 4489 (2012).
7. J. N. Anker, W. P. Hall, O. Lyandres, N. C. Shah, J. Zhao, and R. P. Van Duyne, Nat. Mater. **7,** 442 (2008).
8. A. Y. Elezzabi, K. J. Chau, C. A. Baron, and P. Maraghechi, Opt. Express **17,** 71171 (2009).
9. B. Wood, J. B. Pendry, and D. P. Tsai, Phys. Rev. B **74,** 115116 (2006).
10. W. C. Liu, C. Y. Wen, K. H. Chen, W. C. Lin, and D. P. Tsai, Appl. Phys. Lett. **78,** 685 (2001).
11. B. Jia, H. Shi, J. Li, Y. Fu, C. Du, and M. Gu, Appl. Phys. Lett. **94,** 151912 (2009).
12. H. Gao, H. Shi, C. Wang, C. Du, X. Luo, Q. Deng, Y. Lv, X. Lin , and H. Yao, Opt. Express **13,** 6815 (2005).
13. W. Yu, Y. Fu, L. Li, H. Zhang, H. Liu, Z. Lu, and Q. Sun, Plasmonics **6,** 35 (2011).
14. Y. Wang, W. Srituravanich, C. Sun, and X. Zhang, Proc. SPIE **6324,** 632407 (2006).
15. A. Yanai and U. Levy, Opt. Express **17,** 924 (2009).
16. Z. Liu, J. M. Steele, W. Srituravanich, Y. Pikus, C. Sun, and X. Zhang, Nano Lett. **5,** 1726 (2005).
17. Y. Fu, X. Zhou, and Y. Liu, Plasmonics **5,** 111 (2010).
18. FDTD. Lumerical, http://www.lumerical.com.
19. Z. Liu, J. M. Steele, H. Lee, and X. Zhang, Appl. Phys. Lett. **88,** 171108 (2006).
20. B. H. Cheng, Y.-C. Lan, and D. P. Tsai, Opt. Express **21,** 14898 (2013).
21. Q. Zhan, Adv. Opt. Photon. **1,** 1 (2009).
22. Y. Fu and X. Zhou, Plasmonics **5,** 287 (2010).